Comparative study of Cu2ZnSnSe4 solar cells growth on transparent conductive oxides and molybdenum substrates

S. Temgoua, R. Bodeux, F. Mollica, Negar Naghavi

Comparative study of $Cu_2ZnSnSe_4$ solar cells growth on transparent conductive oxides and molybdenum substrates

S. Temgoua[1], R. Bodeux[1,2], F. Mollica[1] and N. Naghavi[1]

[1] Institut Photovoltaïque d'Ile de France (IPVF), UMR 9006, 30 route départementale 128, 91120 Palaiseau, France

[2] EDF R&D, 30 Route Départementale 128, 91120, Palaiseau, France

Abstract

$Cu_2ZnSnSe_4$ (CZTSe) thin films have been synthetized by cosputtering followed by a selenization treatment on Mo and transparent conductive oxide (TCO) coated soda lime glass substrates, such as ZnO:Al and SnO_2:F (FTO). The aims of the present work is to investigate the impact of the TCO substrates on the CZTSe growth, the reactions at the back contact and the electrical properties of solar cells. The results show that the morphology of CZTSe is affected by the TCO back contacts. It is found that TCO acts as a diffusion barrier of Na from soda lime glass to CZTSe. Thus low incorporation of Na during the annealing could explain the difference in grain size of CZTSe deposited on TCO. Moreover it is evidenced chemical reactions between TCO and CZTSe which affects the interface. While the efficiency up to 8 % is obtained for CZTSe based solar cells deposited on Mo substrate, the efficiency drops to 2.3 % for the solar cells deposited on FTO. The low efficiency is explained by the recombination at the back contact due to the formation of a very thin layer of ZnO at the CZTSe/FTO interface.

I. Introduction

The polycrystalline kesterite $Cu_2ZnSn(S,Se)_4$ (CZTSSe) solar cell is a promising thin-film solar cell technology owing to the abundance of its constitutive elements and its low production cost. Solar cells with a conversion efficiency up to 12.7% has been reported [1]. Most of the CZTSSe based solar cells have been fabricated on Mo substrate which has many advantages (good thermal stability, ohmic contact with CZTSSe) [2,3]. However its opaque nature limits its use as a back contact for semi-transparent, bifacial or tandem solar cells. Thus the use of transparent conductive oxides (TCO) as back contact can offer new possibilities for the application of CZTSSe absorber. The most common TCOs used in chalcogenide solar cells are tin doped indium oxide (In_2O_3:Sn or ITO), fluorine doped tin oxide (SnO_2:F or FTO) or aluminium doped zinc oxide (ZnO:Al).

Many groups have investigated the $Cu(In,Ga)Se_2$ (CIGS) based solar cells deposited on TCO [4-9]. The best efficiencies up to 15.2% are obtained using In_2O_3:Sn (ITO) as back contact [4]. In the case of kesterite based solar cells only very few studies have been reported using this type of back contact. CZTSSe solar cells have been deposited on ITO [10-14] and best efficiencies up to 5.8 % are reached under bifacial illumination [15]. The low efficiency in these solar cells is reported to be due to an interfacial reaction at ITO back contact, which induces the Indium diffusion into the CZTSSe absorber and formation of an oxide SnO_x thin layer, thus degrading the CZTSSe rear interface [12]. CZTSSe based solar cells have also been deposited on FTO [13,16-18], reaching efficiencies up to 7.7% using a Mo nanolayer at the CZTSSe/FTO interface [19]. Lee & al. reported a superstrate CZTSSe based solar cells deposited on ZnO wire and completed with a graphite electrode reaching efficiencies of 1.2 % [20].

In this work, we compared the growth of $Cu_2ZnSnSe_4$ (CZTSe) deposited on two different glass coated TCOs : AZO (ZnO:Al) and FTO. The results are compared to cells with classical Mo back contact [21,22]. The effect of substrate combined with the deposition temperature of the absorber on morphology, composition, crystallinity of CZTSe and the optoelectronic properties of the solar cells will be discussed.

II. Experimental section

Thin Cu-Zn-Sn precursors were deposited on Mo, SnO_2:F (3% of F) (FTO) and ZnO:Al (3% of Al) (AZO) coated soda lime glass substrates using RF magnetron co-sputtering from Cu, Zn and Sn targets at room temperature with [Cu] / ([Sn]+[Zn]) and [Zn] / [Sn] values respectively close to 0.7 and 1.2 (Cu-poor, Zn-rich). These films were then annealed inside a graphite box under a pure selenium atmosphere (Se) provided by an amount of 60 mg of Se pellets. The annealing was done at 600 °C for 15 min [21]. For optoelectronic characterization of the cells, after annealing, a layer of 50 nm of CdS was deposited on the CZTSe absorber by chemical bath deposition and a double layer of ZnO:i / AZO of around 350 nm was deposited by sputtering to complete the solar cell. Before the deposition of the CdS layer, surface etching has been underwent on the CZTSe absorber with KCN, $KMnO_4$+H_2SO_4+Na_2S and $(NH_4)_2S$ [23].

The AZO as back contact was grown on a 3-mm-thick soda-lime glass following the same procedure than the AZO used for the front contact. The layer was deposited by radio-frequency (RF) sputtering using an AZO ceramic target under argon plasma and O_2 flux and at a RF power density of 3W/cm². Two thicknesses of AZO (500 nm and 1300 nm) were compared.

The FTO substrate is a commercially available product from Solems. The FTO layer was deposited by spay pyrolysis on a 2-mm-thick soda-lime glass. Its thickness is 600-700 nm with a roughness of ±40 nm. The sheet resistance of the samples was measured by 4-point probe.

As the CZTSe is annealed at high temperature (500 to 550°C) under Se atmosphere and in order to evaluated the evolution of the TCO parameters under similar conditions, the AZO and FTO layers were also annealed separately. The substrates were placed with 50 mg of Se pellets in the graphite box inserted in a tubular furnace under atmospheric pressure of Ar. A lower amount of Se has been used as ZnO layer is directly in contact with the Se atmosphere. The box was heated at 500°C or 600°C with a linear heating ramp of 15 min, and the temperature was maintained for 45 min.

The composition of the absorber has been studied by Glow discharge optical spectroscopy (GD-OES) measurements. The calibrated signals with a reference give quantitative information of the presence of the elements in the samples. The crystallinity of the absorbers was examined by X-ray diffraction (XRD) with a Panalytical Empyrean X-ray diffractometer using CuK_α radiation (1.5419Å) in the classical Bragg-Brentano and grazing incidence X-ray

diffraction (GIXRD) setups. An incidence angle of 0.5° has been used in order to probes the whole thickness of layers with XRD and to obtain an optimal signal. Raman microprobe measurements were conducted using a HR800-UV Horiba Jobin Yvon spectrometer with 532 nm- and 385 nm lasers and a X50 objective.

In order to characterize the interface between the TCO and the CZTSe absorber, the sample was encapsulated using a transparent epoxy and a 3-mm borosilicate glass and then a lift-off was performed allowing the mechanical separation of the CZTSe layer from the glass/back contact [2,3].

The surface morphology of the samples were investigated by a scanning electron microscopy (SEM) using a Leo Supra 35 field emission gun (FEG) with 15 kV voltage. The electrical properties of the solar cells were characterized by current voltage measurements in dark and light illumination at 25°C (AM1.5 global spectrum). Quantum efficiencies were collected using Oriel IQE-200 ™ instruments.

III. Results and discussions

The chemical, electrical and optical properties of ZnO:Al (AZO) and SnO_2:F (FTO) layers can change during the CZTSe process at high temperature (600 °C) under Se atmosphere. In order to evaluated the evolution of the TCO parameters under similar conditions, The Glass/600-nm-thick AZO, Glass/1300-nm-thick AZO and the Glass/650-nm-thick FTO substrates were placed with 50 mg of Se pellets in graphite box under atmospheric pressure of Ar. The evolution of the square resistance of samples before and after annealing at 500°C and 600°C are presented on Fig.1. The FTO layer seems to be perfectly stable at high temperature as the square resistance remains constant at about 6 Ω/□ whatever the annealing temperature. For the annealing of the 500-nm-thick AZO, both 500 and 600°C under Se atmosphere lead to a dramatically increase of the sheet resistance while annealing of the 1300-nm-thick AZO only moderately increases. Indeed, under the same annealing conditions at 600°C, the sheet resistance is considerably lower for a 1300 nm-thick AZO layer (16 Ω/□) than the 500 nm-thick AZO layer (200 Ω/□). This means that the AZO degradation seems to be a surface effect explaining the lower sheet resistance of the 1300-nm-thick AZO layer.

In order to confirm this hypothesis the crystallinity and the morphology of glass/1300-nm-thick and the Glass/650-nm-thick FTO were analyzed by XRD and SEM measurements

before and after annealing. SEM cross sectional images of FTO and AZO (1300nm) substrates before and after Se annealing are shown in Fig.2. While no change is observed for FTO based samples before and after annealing (Fig.2a and 2b), Fig.2c and 2d reveal morphological changes of AZO induced by the Se annealing. The columnar structure of the AZO layer disappears after annealing under Se and a bilayer of 1000 nm and 500 nm is observed. Moreover, the formation of holes is observed at the interface of the two layers. Differences in lattice parameter between the hexagonal crystal structure of ZnO and the cubic structure of ZnSe, may cause the formation of cavities at the interface between the ZnSe and ZnO layers.

Grazing incidence X-ray diffraction (GIXRD) measurements were performed on FTO and AZO coated substrates before and after annealing at 600°C under Se atmosphere. Fig.3 confirms that FTO is quite stable under Se atmosphere, as the XRD diagrams are exactly the same before and after annealing.

It is also observed that the (103)/(002) ratio of ZnO increases from 1.3 before annealing to 2.6 after annealing. In parallel the (103)/(102) ratio of ZnO increases from 6.7 before annealing to 7.6 after annealing. Based on these results it appears that there is change on the preferential orientation of ZnO after annealing.

Moreover several new peaks in addition to ZnO peaks are observed after annealing which are assigned to ZnSe phase (PDF # 00-037-1463) confirming the formation of a thin ZnSe layer at the surface of the film as observed on SEM pictures (Fig.2d). The formation of ZnSe could result from substitution of oxygen with selenium. Reaction of oxides phases with chalcogenide phases through substitution of oxygen by the chalcogen (S, Se) have already been studied in previous works [24,25].

During the annealing, the transparent conducting back contact is not only in contact with Se but also with the CZTSe phase and in consequently with its associated binaries. The reactivity of the binaries with the TCO back contact can be estimated by the calculation of the standard Gibbs free energy of the reaction (ΔG_f). Table 1 summarizes the ΔG_f of different reactions potentially occurring at the interface between the TCO and the CZTSe absorber [26]. If $\Delta G_f < 0$, the reaction is thermodynamically favored. The CZTSe decomposition is not possible if any reaction with the constituent binaries (Cu_2Se, Sn_2Se_3, ZnSe) is thermodynamically not allowed.

For the AZO back-contact, the calculated ΔG_f for the reaction between ZnO and Se is negative. Therefore, ZnSe layer can be formed at the interface between the CZTSe and the AZO. The reaction of ZnO with the Se vapors leads to the emission of SeO_2 gas.

On the opposite, for the FTO back-contact, the calculated ΔG_f calculated for the reactions between SnO_2 and Se, and Cu_2Se are positive. Thus FTO would not react during the CZTSe formation. The CZTSe process is likely to impact the AZO layer performance leading not only to a reduction of the doping concentration but also to some thermodynamically favored reactions between CZTSe and AZO. On the opposite, the FTO layer is perfectly stable up to 600°C. However, it is important to note that the kinetic of the reaction may be too long and that the annealing process is not at thermodynamically equilibrium. Therefore, the experimental results can differ from the conclusions based on these calculations.

SEM analysis of CZTSe absorber deposited on Mo, AZO, and FTO are shown in Fig.4. The films are dense whatever the substrate. However, the morphology of grains depends to the back contact. Indeed, while larger grains of CZTSe > 2µm are formed on Mo substrate (Fig.4a), smallest grains (< 1 µm) are formed on FTO and AZO substrates (Fig.4b and 4c, respectively). More particularly, in the case of AZO coated substrate, voids are observed at the interface between CZTSe and AZO. The voids could be attributed to the reaction between Se and ZnO during the annealing to form the thin ZnSe layer and the emission of SeO_2 gas in agreement with the Fig.2. Thus SeO_2 diffusion into the CZTSe layer could degrades the interface.

The distribution of the chemical elements through the absorber layers deposited on Mo, FTO and AZO, obtained by GD-OES, are shown in Fig.5. For Mo and FTO coated substrates (Fig.5a and 5b, respectively), the profiles of Cu, Zn, Sn and Se are homogeneous throughout the thickness in agreement with the literature [13]. As observed in SEM pictures (Fig. 4d) the interface between CZTSe and FTO is rough. The interface roughness broadens the observed elemental profiles in GDOES. Moreover, as the Sn is both in the coating and in the substrate layer, it is not obvious to get a sharp interface between CZTSe and FTO and a gradual increase of Sn and O at the back side is observed while Cu, Zn and Se decreases. As shown by the thermodynamic calculations, FTO is quite stable at these temperatures confirming that the gradual increase of Sn and O at the CZTSe/FTO is not caused by the diffusion of Sn from FTO into CZTSe.

For the AZO coated substrate (Fig. 5c), the profiles of Cu and Sn appear relatively homogenous. However, the profiles of Zn and Se strongly vary through the thickness. Indeed, a segregation of Zn is visible at the back side. It seems that the composition of the substrate considerably modify the growth of CZTSe and especially its Zn content.

To highlight the impact of the AZO and FTO on the Na diffusion, the Na concentration in the CZTSe layer was also estimated by GD-OES. The standard Mo substrate allows the Na diffusion from the soda-lime glass to the CZTSe through the Mo layer. However the Na intensity for CZTSe on FTO and AZO back-contact are closed to 0, meaning that both FTO and AZO back-contacts hinder the diffusion of Na. The low diffusion of Na through TCO, in particular AZO and FTO has been evidenced on CIGSe based solar cells [8,27-29].

XRD patterns of CZTSe absorbers deposited on Mo, FTO and AZO are shown in Fig.6. The signature of Mo, FTO and AZO layers are visible. Moreover, the main reflections (112) at 27.29°, (220) at 45.28°, and (312) at 53.64° of the CZTSe phase are clearly observed whatever the substrate [21]. For the Mo coated substrate, the $SnSe_2$ secondary phase (PDF 089-3197) are also visible (Fig.6a) [30]. The (112) orientation of CZTSe is shown on a short range in the inset part of Fig.6. FWHM of (112) peak is sharper for CZTSe deposited on Mo and FTO than the one on AZO indicating a higher crystalline quality of CZTSe phase. These results are in agreement with the previous results in Fig.4 and 5 which show the disrupted growth of CZTSe deposited on AZO.

Due to the similar crystal structures of the ZnSe and Cu_2SnSe_3 with CZTSe phases, it is not possible to conclude on the basis of X-ray measurements whether CZTSe if clearly formed. Thus, Raman spectroscopy is used to identify it. Raman spectra obtained with a 532 nm-laser wavelength of CZTSe films deposited on the different substrates Mo, FTO and AZO are shown in Fig.7a. Raman spectroscopy confirms the formation of the CZTSe phase on the different coated substrates.

It is important to note that even if SEM and XRD analysis have identified a thick ZnSe layer at the surface of AZO (Fig.2b, Fig. 3) after annealing, no ZnSe signal is observed for the CZTSe/AZO stack. In fact, the penetration depth of Raman spectroscopy is some hundreds of nanometers. Thus Raman spectroscopy cannot detect the signal of ZnSe at the interface between CZTSe and AZO.

Moreover, an additional peak attributed to the $SnSe_2$ phase is visible on the surface of CZTSe film deposited on FTO while it has not been detected by XRD. $SnSe_2$ is not a continuous film and could escape from the Raman and XRD analysis [30]. These complementary results show

that the $SnSe_2$ phase appears whatever the substrate and only depends on the growth conditions of CZTSe.

In order to access the interface between CZTSe and the TCO layer, lift-off technique has been used. However lift-off has been unsuccessful for CZTSe deposited on AZO. Fig.7b shows the Raman spectra of FTO coated substrate using UV laser wavelength after lift-off of CZTSe. FTO coated substrate before the CZTSe deposition is shown as reference. The FTO phase is observed and corresponds to the peak centered at 636 cm^{-1} [31]. FTO coated substrate after lift-off reveals the presence of a secondary phase with 2 peaks at 568 cm^{-1} and 1142 cm^{-1}. This secondary phase fully absorbs UV laser wavelength and the peak of FTO centered at 636 cm^{-1} is no longer visible. These 2 peaks are attributed to the 1st and 2nd order vibrations of the ZnO phase [32].

As Zn can be only provided by CZTSe layer, the ZnO phase at the interface between CZTSe and FTO could indicate the decomposition of CZTSe which provides the Cu, Zn and Sn elements. Thus the reaction of these elements with oxygen coming from FTO could product binary oxides. However, no additional secondary phases, such as Cu_xO has been observed.

The formation of oxide secondary phases at the interface between chalcogenide and TCO has been observed in previous works. For example, for CIGSe films deposited on ITO, the presence of a Ga_2O_3 resistive layer is reported [4,7] forming an electrical barrier for carrier transport [27,28]. For CZTSe films deposited on ITO, the formation of SnO_2 phases is reported. However, the effect of SnO_2 on the electrical properties of solar cells has been found negligible [12,18].

In order to assess the impact of the back contact on the electrical properties of solar cells IV measurements are performed on completed cells. Unfortunately all solar cells were shunted in the case of AZO/CZTSe based solar cells. In Fig.8.a, I-V curves for the best solar cells deposited on Mo/glass and FTO/glass substrates are reported. Their electrical parameters are summarized in Table 2. It can be found that all the electrical parameters of the solar cells deposited on FTO are lower than the ones deposited on Mo. For CZTSe absorbers deposited on Mo, the best solar cells have led to efficiencies up to 8.0 % [21,22]. The best efficiency of solar cells on FTO back contact is about 2.3%. The solar cells deposited on FTO suffer from a low FF, J_{sc} and V_{oc}. In fact, I-V characteristics under illumination of the solar cells deposited on FTO exhibits a slight slope at 0 V which shows that the solar cell has a current collection that depends on the voltage. The slope is higher under illumination than in the dark indicating the presence of recombination. It is well known that absence of Na is detrimental for the CZTSe cell (low doping concentration or high defect density), and the Na has to be supplied

by an external source. Moreover the back contact/CZTSe interface is the p-contact of the cell and has to be ohmic [19]. It has been shown that when the CZTSe is grown directly on FTO, an ohmic contact is achieved. However, the series resistances of the cells are slightly higher than the reference cells on Mo substrate. In our case a rectifying behavior is observed either due to the formation of a pn-junction between the n-type TCO and the p-type CZTSe or due to the high contact resistance of the ZnO secondary phase at the CZTS/SnO_2 interface. In fact ZnO is generally n-doped and therefore degrades the performance of the cell.

Fig.8b shows the EQE of the best solar cells deposited on Mo and FTO. The EQE spectrum exhibits a maximum around 560 nm at a level about 80% whatever the substrate. However, EQE drastically decreases with the wavelengths from 600 nm to 1200 nm for FTO coated substrate in contrary to Mo coated substrate. Integrated Jsc from EQE, obtained for the both solar cells, are 32.02 mA/cm^2 and 21.5 mA/cm^2 for CZTSe/Mo and CZTSe/FTO, respectively. These values are slightly higher than the ones obtained by I-V analysis. Low EQE is correlated with a low collection efficiency of the absorber, such as the losses at highest wavelengths in the near IR region could also be due to a recombination rate raised to the back contact [33,34]. Thus, several reasons can be reported to understand the low efficiency of CZTSe solar cell on FTO. On the one hand, in the case of Mo back contact, the formation of $MoSe_2$ at the CZTSe / Mo interface forms an ohmic contact. Thus, low recombination rate contributes to increase Voc, Jsc and FF. In the case of FTO back contact, high recombination rate comes from defects at the contact between CZTSe and FTO. In fact, ZnO secondary phases or diffusion of the oxygen to CZTSe could damage the interface. On the other hand, it has been observed that the TCO prevents the diffusion of Na through CZTSe. The diffusion of Na through CZTSe has a beneficial effect on doping concentration and defect density of the absorber. Thus, the improvement of the interface quality between CZTSe and FTO could also increase Voc and FF [28, 35-37].

IV. Conclusion

CZTSe based solar cells deposited on Mo, ZnO:Al (AZO), and SnO_2:F (FTO) coated substrate have been studied. It has been found that the annealing temperature under Se has no impact on the FTO substrate up to 600°C, whereas the temperature should remain below 500°C for the 1300-nm-thick AZO. During the CZTSe deposition, FTO substrate is the most stable: no reaction are thermodynamically favored between the CZTSe phases and FTO.

281 However, CZTSe decomposition reaction is thermodynamically possible at the ZnO interface
282 with the formation of a ZnSe phase. Moreover both FTO and AZO layer hinder the Na
283 diffusion from the glass to the CZTSe absorbers leading to a lack of Na compared to the
284 standard Mo substrate. Thus Solar cells based on CZTSe were made with an efficiency of
285 2.3% on FTO while solar cells CZTSe deposited on Mo up to 8.0 %. Low efficiency of
286 CZTSe solar cell on FTO coated substrate suffers of recombination at the back contact which
287 limits Voc, Jsc and FF. Low efficiency has been explained by the presence of the ZnO
288 secondary phase at the back contact and the low diffusion of Na through CZTSe.

289

290 References

291

292 [1] J. Kim, H. Hiroi, T. K. Todorov, O. Gunawan, M. Kuwahara, T. Gokmen, D. Nair, M.
293 Hopstaken, B. Shin, Y. S. Lee, W. Wang, H. Sugimoto, et D. B. Mitzi, « High Efficiency
294 $Cu_2ZnSn(S,Se)_4$ Solar Cells by Applying a Double In_2S_3/CdS Emitter », Adv. Mater., 26
295 (2014) 7427- 7431.
296 [2] S. Temgoua, R. Bodeux, N. Naghavi, "A better understanding of the reaction pathways in
297 the formation of Cu2ZnSn(Sx,Se1−x)4 thin films", Solar Energy Materials and Solar Cells
298 172 (2017) 160.

299 [3] S. Temgoua, R. Bodeux, N. Naghavi, "Influence of the annealing atmosphere and
300 precursor's thickness on the properties of CZTSSe based solar cells" Solar Energy Materials
301 and Solar Cells 191 (2019) 123-132
302 [4] T. Nakada, Y. Hirabayashi, T. Tokado, D. Ohmori and T. Mise, « Novel device structure
303 for Cu(In,Ga)Se_2 thin film solar cells using transparent conducting oxide back and front
304 contacts », Sol. Energy, 77, 6, (2004) 739- 747.
305 [5] D. L. Young, J. Abushama, R. Noufi, X. Li, J. Keane, T. A. Gessert, J. S. Ward, M.
306 Contreras, M. Symko-Davies, and T. J. Coutts, "A new thin-film $CuGaSe_2$/Cu(In,Ga)Se_2
307 bifacial, tandem solar cell with both junctions formed simultaneously," in Conference Record
308 of the Twenty-Ninth IEEE Photovoltaic Specialists Conference, 2002, pp. 608–611, May
309 2002.

310 [6] S. Nishiwaki, S. Siebentritt, P. Walk, and M. Ch. Lux-Steiner, "A stacked chalcopyrite
311 thin-film tandem solar cell with 1.2 V open-circuit voltage," Progress in Photovoltaics :
312 Research and Applications, 11 (2003) 243–248.

313 [7] T. Nakada, "Microstructural and diffusion properties of CIGS thin film solar cells
314 fabricated using transparent conducting oxide back contacts," Thin Solid Films, 480 (2005)
315 419.

316 [8] F. Mollica, M. Jubault, F. Donsanti, A. Loubat, M. Bouttemy, A. Etcheberry, N. Naghavi,
317 "Light management in ultra-thin CIGS solar cells by substituting the back contact with a
318 TCO-based reflector", Thin Solid films, 633 (2017), 202-207.

[9] L. Gouillart, A. Cattoni, J. Goffard, F. Donsanti, G. Patriarche, M. Jubault, N. Naghavi, S. Collin "Development of reflective back contacts for high-efficiency ultrathin Cu(In,Ga)Se2 solar cells", Thin Solid Film 672 (2019) 1–6.

[10] J. Ge, J. Chu, J. Jiang, Y. Yan, and P. Yang "Characteristics of In-Substituted CZTS Thin Film and Bifacial Solar Cell" ACS Appl. Mater. Interfaces, 6 (2014) 21118−21130.

[11] J. Ge, J. Chu, Y. Yan, J. Jiang and P. Yang, « Co-electroplated Kesterite Bifacial Thin-Film Solar Cells: A Study of Sulfurization Temperature », ACS Appl. Mater. Interfaces, 7 (2015) 10414-10428.

[12] J. Ge, J. Chu, J. Jiang, Y. Yan, and P. Yang, "The Interfacial Reaction at ITO Back Contact in Kesterite CZTSSe Bifacial Solar Cells," ACS Sustainable Chemistry & Engineering, 3 (2015) 3043–3052.

[13] J.S. Kim, J.K. Kang, and D.K. Hwang, "High efficiency bifacial $Cu_2ZnSnSe_4$ thin-film solar cells on transparent conducting oxide glass substrates", APL Materials 4 (2016) 096101.

[14] J.S. Kim, J.K. Kang and D.K. Hwanga, "Efficiency enhancement of bifacial $Cu_2ZnSnSe_4$ thin-film solar cells on indium tin oxide glass substrates by suppressing In-Sn diffusion with Mo interlayer" Journal of Power Sources 400 (2018) 9–15.

[15] J. Ge, Y.Yu, W. Ke, J. Li, X. Tan, Z. Wang, J. Chu, and Y. Yan, "Improved Performance of Electroplated CZTS Thin-Film Solar Cells with Bifacial Configuration" ChemSusChem, 9 (2016) 2149.

[16] P. K. Sarswat and M. L. Free, "Demonstration of a sol–gel synthesized bifacial CZTS photoelectrochemical cell," physica status solidi (a), 208 (2011) 2861– 2864.

[17] P. K. Sarswat and M. L. Free, « A Comparative Study of Co-electrodeposited Cu_2ZnSnS_4 Absorber Material on Fluorinated Tin Oxide and Molybdenum Substrates », J. Electron. Mater., 41 (2012) 2210-2215.

[18] J. Henry, K. Mohanraj and G. Sivakumar, "Vacuum evaporated FTO/$(Cu,Ag)_2ZnSnSe_4$ thin films and its electrochemical analysis", Vacuum, 160 (2019) 347-354.

[19] M. Espindola-Rodriguez, D. Sylla, Y. Sánchez, F. Oliva, S. Grini, M. Neuschitzer, L. Vines, V. Izquierdo-Roca, E. Saucedo, and M. Placidi, "Bifacial kesterite solar cells on FTO substrates" ACS Sustainable Chem. Eng. 2017, 5, 12, 11516-11524.

[20] D. Lee, "Solution-processed CZTS superstrate solar cell using vertically aligned

ZnO nanorods" Nanotechnology, 25 (2014) 065401.

[21] R. Bodeux, F. Mollica and S. Delbos, « Growth of $Cu_2ZnSnSe_4$ by cosputtering and reactive annealing atmosphere », Sol. Energy Mater. Sol. Cells, 132 (2015) 6773.

[22] R. Bodeux, J. Rousset, F. Tsin, F. Mollica, E. Leite, S. Delbos, "Determination of the electronic properties of $Cu_2ZnSnSe_4$ based solar cells by impedance spectroscopy and current–voltage characteristics analysis" Applied Physics A 124 (2018) 22.

[23] T. Olar, I. Lauermann, H. Xie, M. Neuschitzer, E. Saucedo, W. Calvet, A. Steigert, B. Ümsür, B. Chacko, V. Parvan, M. Gorgoi, B. Senkovskiy and M.L. Steiner," Assessment of chemical and electronic surface properties of the $Cu_2ZnSn(S,Se)_4$ after different etching procedures by synchrotron-based spectroscopies" Energy Procedia 84 (2015) 8 – 16.

[24] T. Tsirlina, "Growth of crystalline WSe_2 and WS_2 films on amorphous substrate by reactivee (Van Der Waals) rheotaxy," Solar Energy Material & Solar Cells, 44 (1996) 457.

[25] D. Lee and K. Yong, "Partial conversion reaction of ZnO nanowires to ZnSe by a simple selelenization method and their photocatalytic activities," Materials Chemistry and Physics, 137 (2012) 194–199.

[26] F. Mollica, "Optimization of ultra-thin $Cu(In,Ga)Se_2$ based solar cells with alternative back-contacts" PhD thesis, University of Pierre et Marie Curie, France, 2016.

[27] F.-J. Haug, "Characterization of $CuGa_2$/ZnO for superstrate solar cells," Thin Solid Films, 361 (2000) 293.

[28] F.-J. Haug, "Comparison of structural and electrical properties of Cu(In,Ga)Se2 for superstrate and substrate solar cells," Thin Solid Films, 403 (2002) 293.

[29] T. Prabhakar and N. Jampana, "Effect of sodium diffusion on the structural and electrical properties of Cu_2ZnSnS_4 thin films" Solar Energy Materials and Solar Cells, 95 (2011) 1001-1004.

[30] S. Temgoua, R. Bodeux, N. Naghavi, et S. Delbos, « Effects of $SnSe_2$ secondary phases on the efficiency of $Cu_2ZnSn(Sx,Se_{1-x})_4$ based solar cells », Thin Solid Films, 582 (2015) 215219.

[31] Z. W. Chen, J. K. L. Lai, and C. H. Shek, "Insights into microstructural evolution from nanocrystalline SnO_2 thin films prepared by pulsed laser deposition," Physical Review B, 70 (2004) 165314.

379 [32] N. Xu, Y. Cui, Z. Hu, W. Yu, J. Sun, N. Xu, and J. Wu, “Photoluminescence and low-
380 threshold lasing of ZnO nanorod arrays,” Optics Express, 20 (2012) 14857–14863.

381 [33] S. Siebentritt, “What limits the efficiency of chalcopyrite solar cells ?,” Solar Energy
382 Materials and Solar Cells, 95 (2011) 1471–1476.

383 [34] L. Guo, Y. Zhu, O. Gunawan, T. Gokmen, V. R. Deline, S. Ahmed, L. T. Romankiw, and
384 H. Deligianni, “Electrodeposited Cu2ZnSnSe4 thin film solar cell with 7% power conversion
385 efficiency,” Progress in Photovoltaics : Research and Applications, 22 (2014) 58-68.

386 [35] J. V. Li, D. Kuciauskas, M. R. Young, and I. L. Repins, “Effects of sodium incorporation
387 in Co-evaporated $Cu_2ZnSnSe_4$ thin-film solar cells,” Applied Physics Letters, 102, (2013)
388 163905–163905–4.

389 [36] A. Nagaoka, H. Miyake, T. Taniyama, K. Kakimoto, Y. Nose, M. A. Scarpulla, and K.
390 Yoshino, “Effects of sodium on electrical properties in Cu_2ZnSnS_4 single crystal,” Applied
391 Physics Letters, 104 (2014) 152101.

392 [37] T. Gershon, B. Shin, N. Bojarczuk, M. Hopstaken, D. B. Mitzi, and S. Guha, “The Role
393 of Sodium as a Surfactant and Suppressor of Non-Radiative Recombination at Internal
394 Surfaces in Cu_2ZnSnS_4,” Advanced Energy Materials, 5 (2015) 1400849.

395 Table

396

397 **Table 1** Gibbs free energy of the potential reactions at the CZTS/back-contact.

Reaction equation	Gibbs free energy at 500°C Reaction equation per mol of Mo, ZnO or SnO_2 *ΔGf* (kJ/mol)
$Mo+Se_2 = MoSe_2$	**-153**
$2ZnO+1.5Se_2(g) = 2\ ZnSe + SeO_2\ (g)$	**-30**
$Cu_2Se + ZnO = Cu_2O + ZnSe$	**87**
$CuSe + ZnO = CuO + ZnSe$	**63**
$SnO_2 + 1.5Se_2(g) = SnSe_2 + SeO_2(g)$	**176**
$SnO_2 + Se_2(g) = SnSe(g) + SeO_2(g)$	**286**
$2Cu_2Se + SnO_2 = 2Cu_2O + SnSe_2$	**287**
$2CuSe + SnO_2 = 2CuO + SnSe_2$	**241**

398

399 **Table 2** Electrical parameters of CZTSe based solar cells deposited on Mo/glass and
400 FTO/glass

	Voc (mV)	Jsc (mA/cm^2)	FF (%)	Eff (%)	Eg (eV)
CZTSe/Mo	460	28.6	61	8.0	1.03
CZTSe/FTO	290	18.6	43	2.3	1.07

401

402

403 Figures

404

405 **Figure 1** Sheet resistances of AZO(500 nm), AZO(1300 nm), and FTO before and after
406 annealing at different temperature under Se atmosphere for 45 min

407

408 **Figure 2** SEM morphologies of as deposited a) AZO, b) FTO and annealed c) AZO, d) FTO
409 at 600°C for 45 min under Se atmosphere

410

411 **Figure 3** GIXRD patterns of a) FTO and b) AZO before and after annealing at 600°C under
412 Se atmosphere for 45 min

413

414 **Figure 4** SEM morphologies of CZTSe absorber deposited on a), b) Mo, c),d) FTO et e),f)
415 AZO

416

417 **Figure 5** GD-OES composition profiles for CZTSe deposited on a) Mo, b) FTO and c) AZO

418

419 **Figure 6** XRD patterns of CZTSe films deposited on Mo, AZO and FTO

420

421 **Figure 7** Raman spectra of a) CZTSe deposited on different substrates Mo, FTO and AZO at
422 532 nm and b) FTO substrate at 325 nm laser wavelength before CZTSe deposition and after
423 lifted off CZTSe

424

425 **Figure 8** J(V) curves of CZTSe based solar cells deposited on Mo/glass and FTO/glass

Figure 1
Click here to download high resolution image

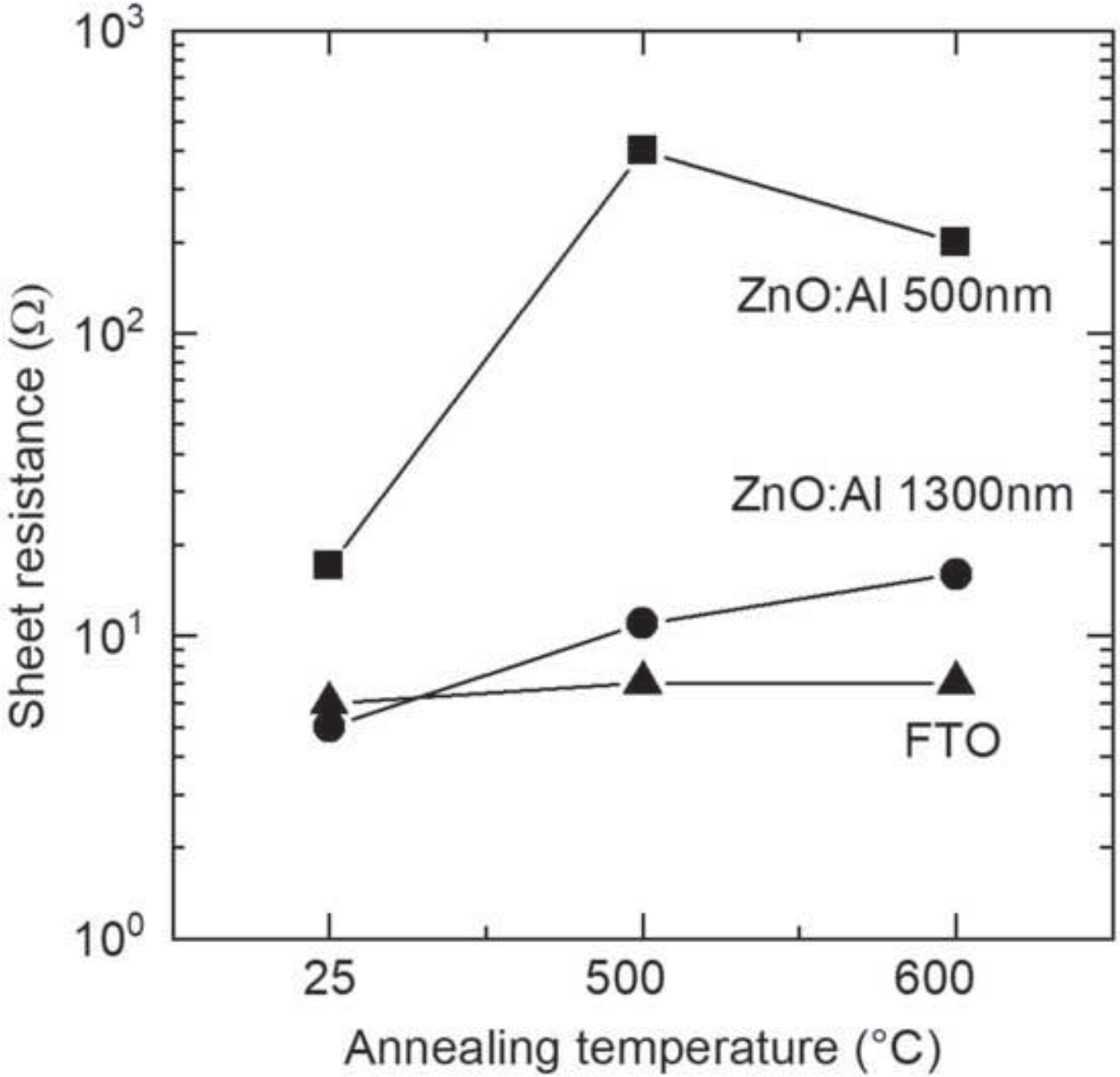

Figure 2

Click here to download high resolution image

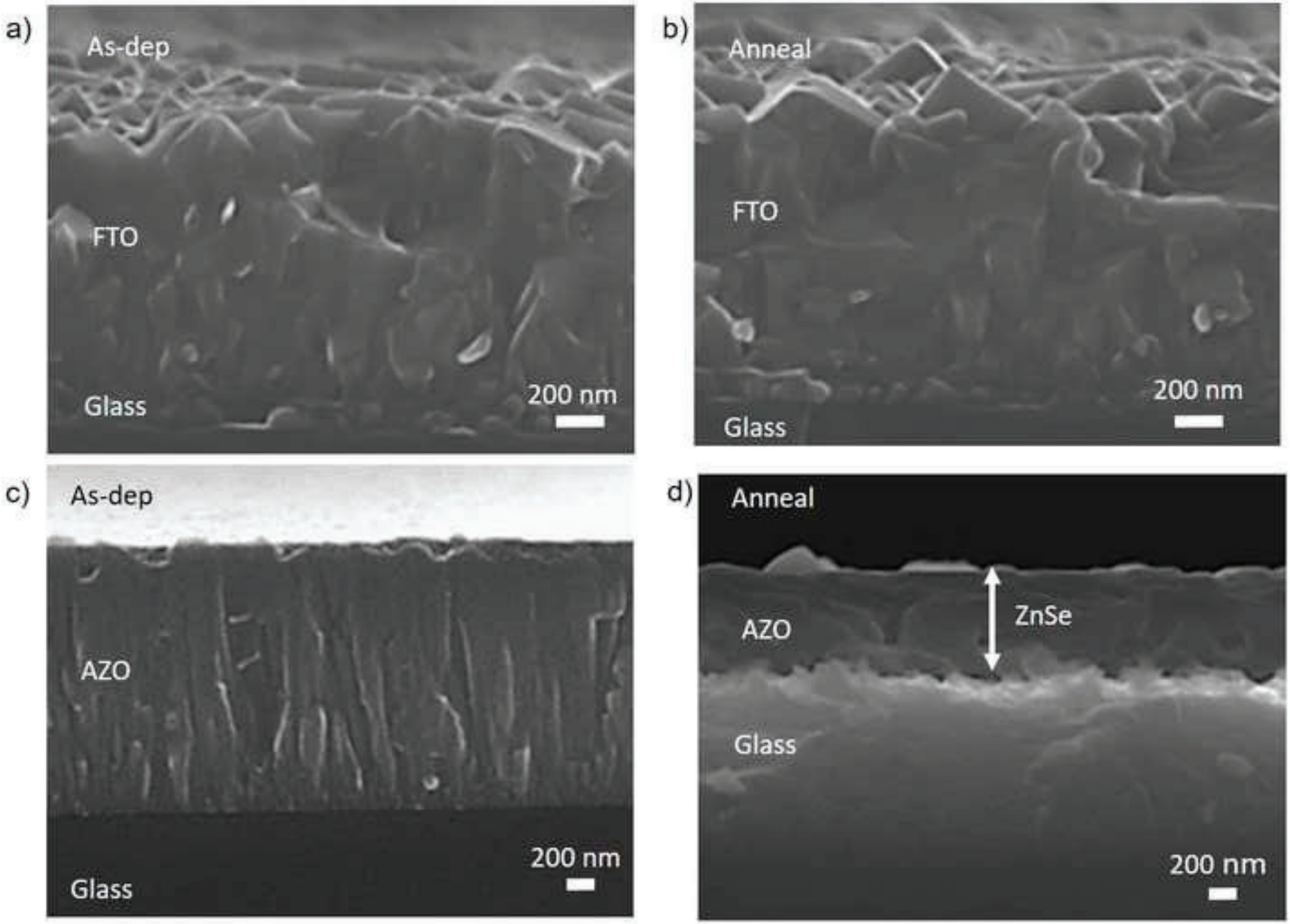

Figure 3
Click here to download high resolution image

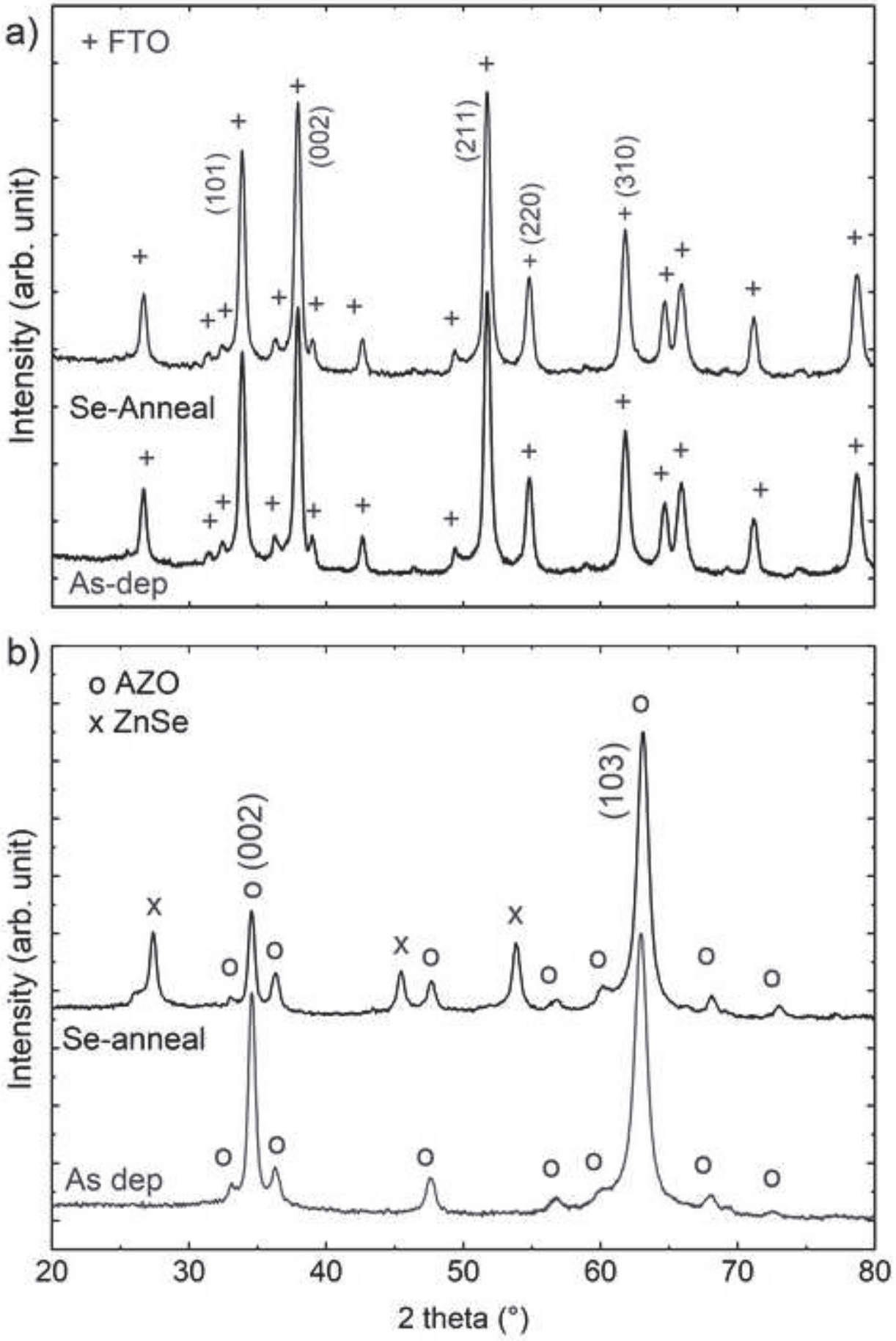

Figure 4

Click here to download high resolution image

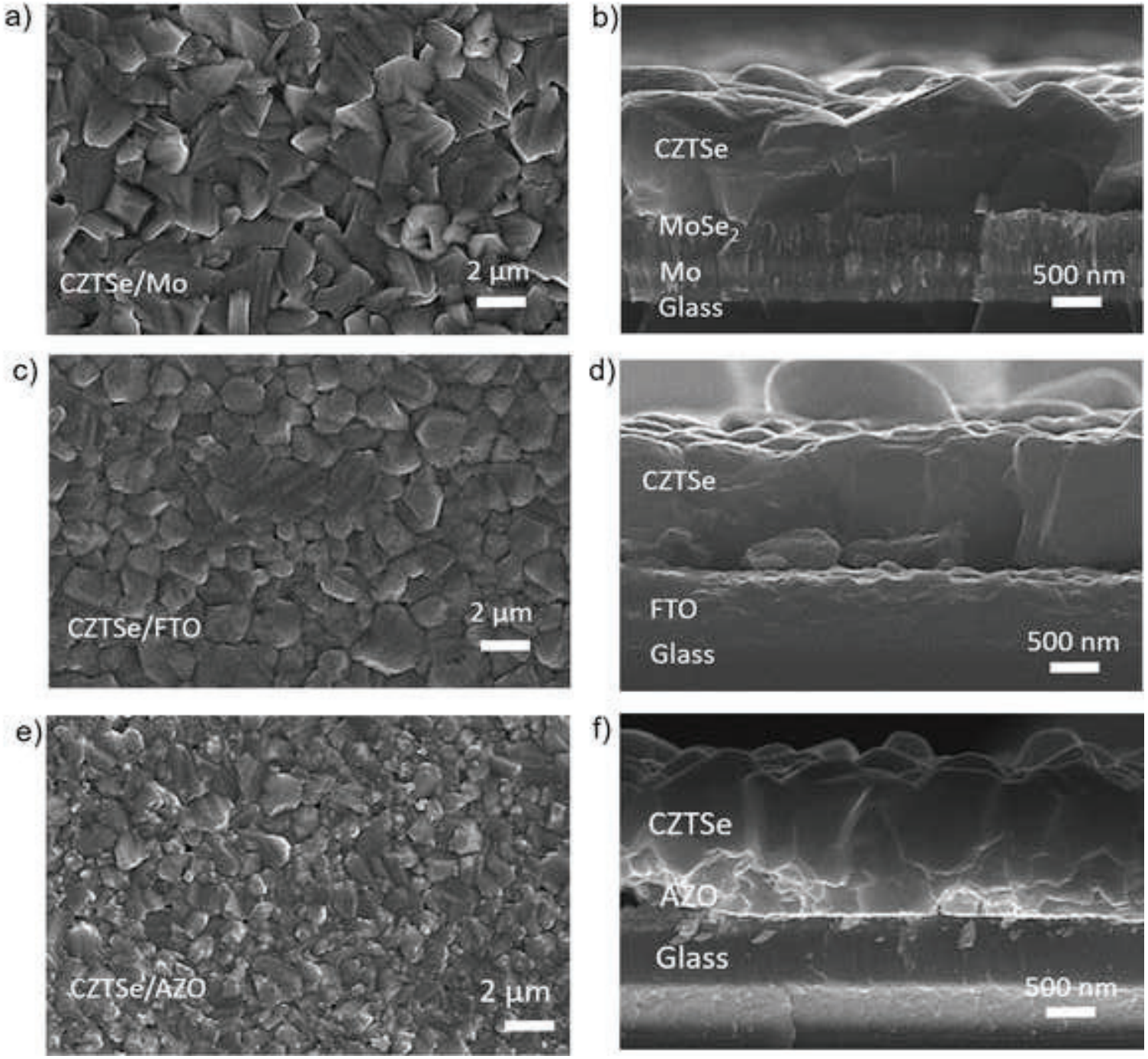

Figure 5
Click here to download high resolution image

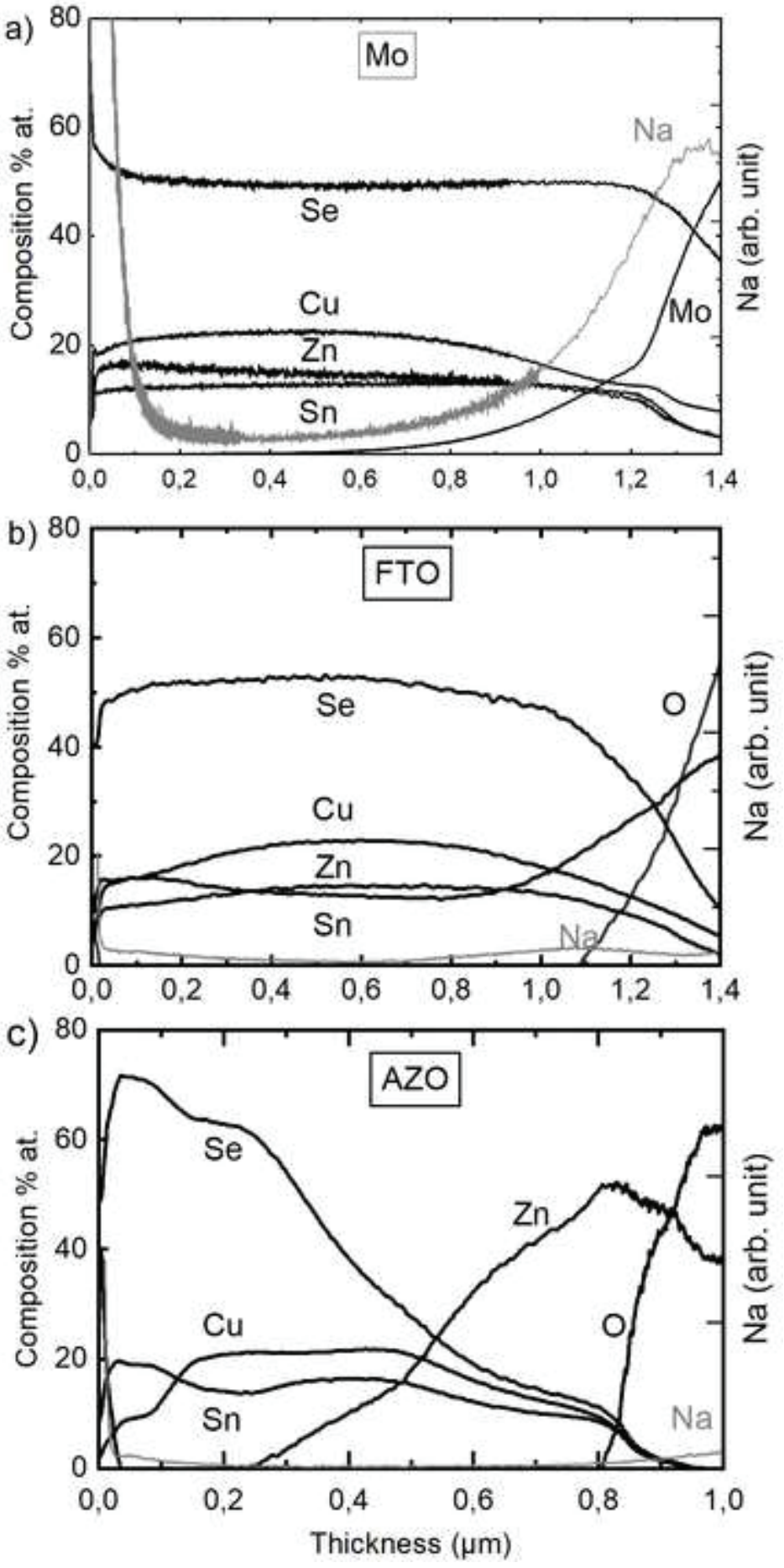

Figure 6
Click here to download high resolution image

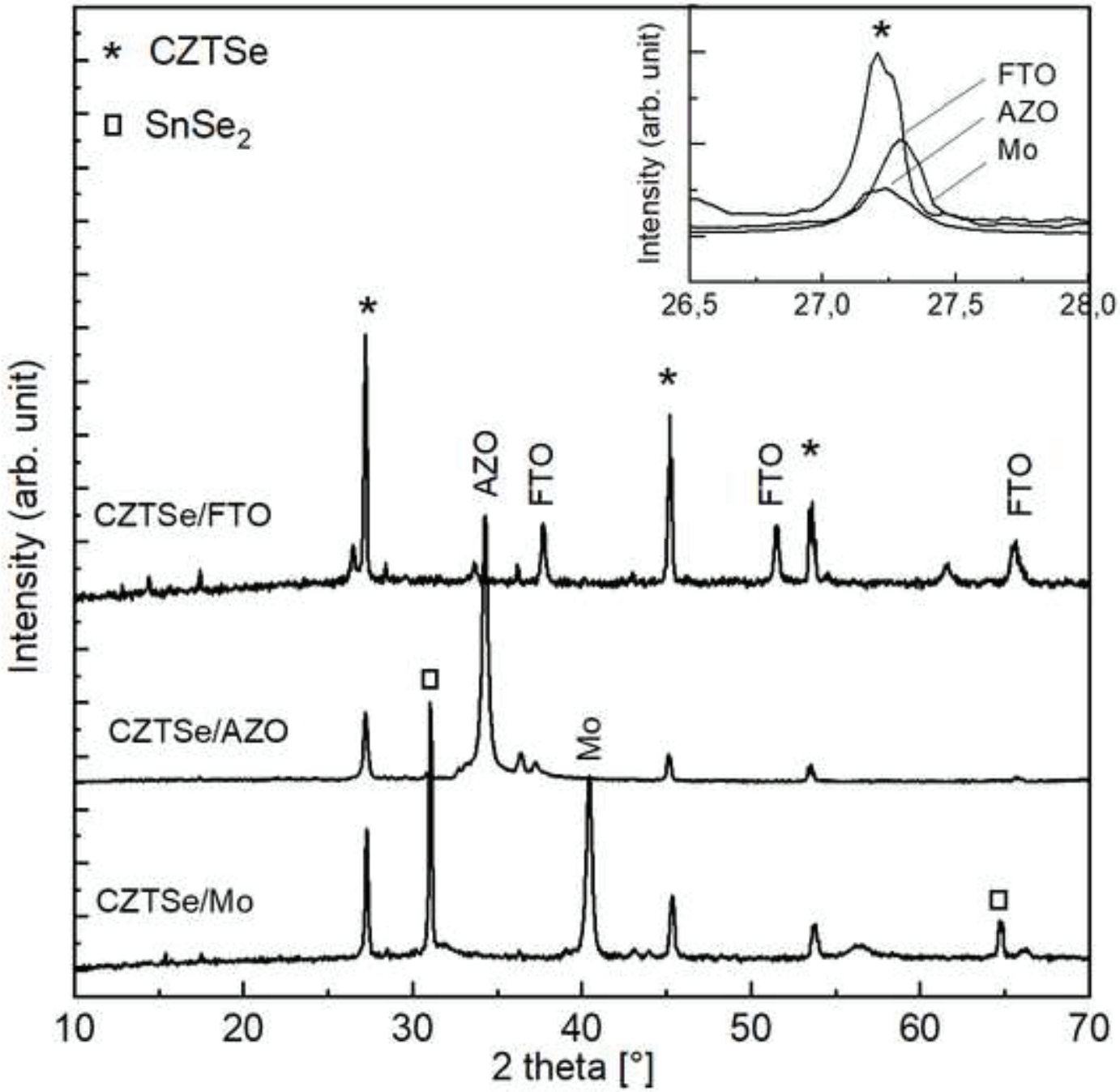

Figure 7
Click here to download high resolution image

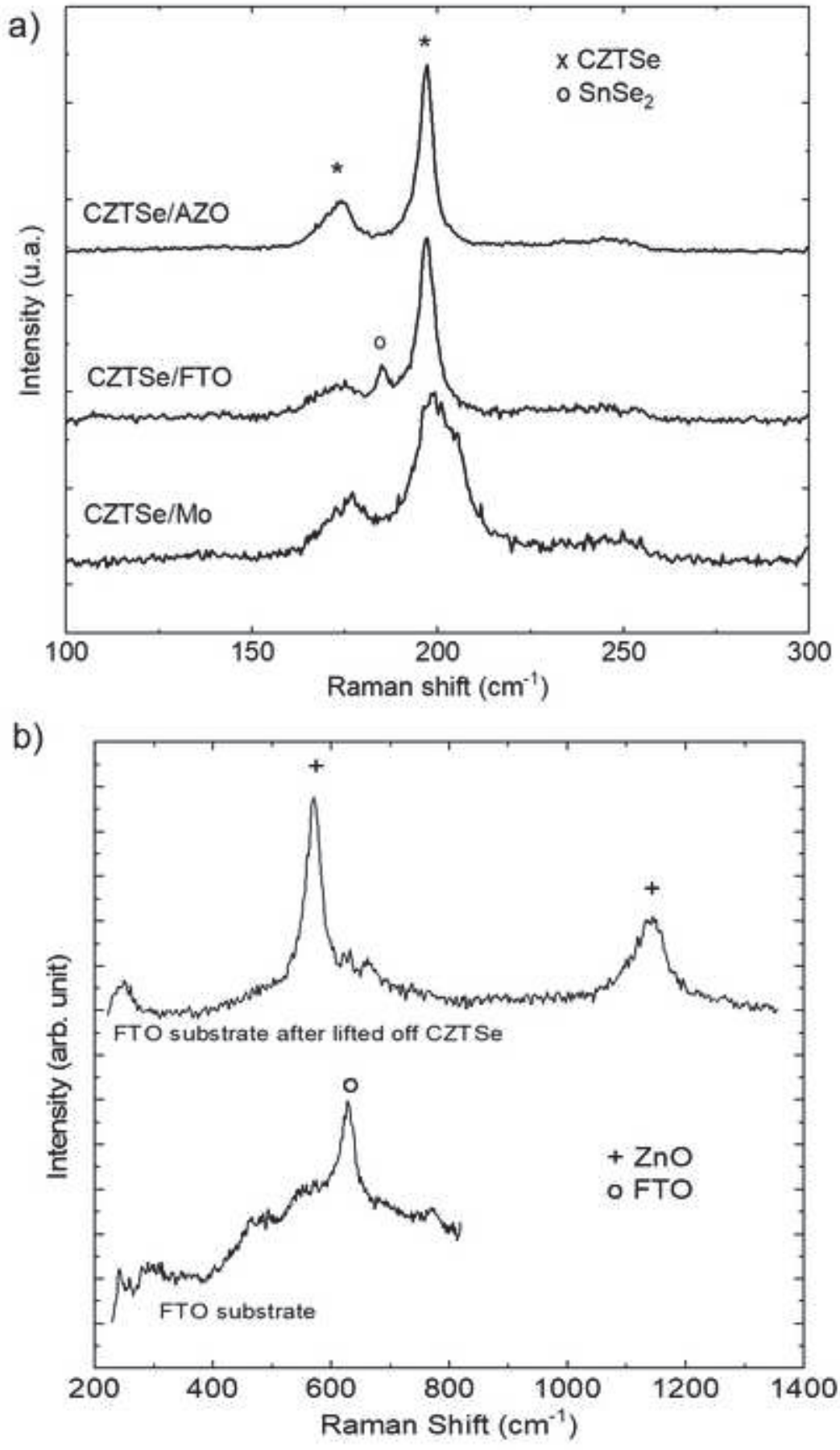

Figure 8
Click here to download high resolution image